Dose reduction in CT by anatomically adapted tube current modulation. I. Simulation studies

Michael Gies, Willi A. Kalender,[a] Heiko Wolf, and Christoph Suess
Institute of Medical Physics, University of Erlangen-Nuremberg, Krankenhausstr. 12, D-91045 Erlangen, Germany

Mark T. Madsen
Department of Radiology, University of Iowa, Iowa City, Iowa 12345

(Received 10 December 1998; accepted for publication 26 July 1999)

Tube current modulation governed by x-ray attenuation during CT (computed tomography) acquisition can lead to noise reduction which in turn can be used to achieve patient dose reduction without loss in image quality. The potential of this technique was investigated in simulation studies calculating both noise amplitude levels and noise distribution in CT images. The dependence of noise on the modulation function, amplitude of modulation, shape and size of the object, and possible phase shift between attenuation and modulation function were examined. Both sinusoidal and attenuation-based control functions were used to modulate tube current. Noise reduction was calculated for both ideal systems and for real systems with limited modulation amplitude. Dose reductions up to 50% can be achieved depending on the phantom geometry and tube current modulation function. Attenuation-based tube current modulation yields substantially higher reduction than fixed-shape modulation functions. Optimal results are obtained when the current is modulated as a function of the square root of attenuation. A modulation amplitude of at least 90% should be available to exploit the potential of these techniques. © *1999 American Association of Physicists in Medicine*. [S0094-2405(99)03011-4]

Key words: computed tomography (CT), dose, tube current modulation, simulation studies

I. INTRODUCTION

Patient dose values in CT are relatively high when compared to standard radiological exams. Because of their increasingly frequent use, CT examinations contribute a substantial portion to the total radiation exposure of the population from medical applications.[1,2] Dose reduction has always been a major concern for medical and health physicists. Their role has often been limited to advising on the appropriate choice of scan parameters since changes on the complex CT apparatus have not been easy to accomplish. Reducing patient dose by simply lowering tube current has been suggested by several investigators.[3–5] This approach increases image noise which often deteriorates low contrast detectability.[6] A more sophisticated method adapts the tube current to x-ray attenuation as it changes with projection angle.[7] The basic idea is to lower tube current only for projections associated with low attenuation.

A system based on this principle is available commercially[8] and is often referred to as ''Smart Scan.'' Two localizer radiographs for lateral and a.p. direction are taken initially to estimate the minimum and maximum attenuation; tube current is then modulated sinusoidally based on this information. Modulation amplitude has been limited to a tube current reduction of 50%. These efforts were a decisive stimulus for the work presented below.

Using simulations, we investigated several variations of the approach to modulate the tube current for a 360° scan. We followed a general approach using different modulation functions and investigated various object cross sections and constraints to determine optimal settings. Simulations were the optimal tool to start these investigations. Arbitrary modulation functions could be used that would be difficult to implement on an actual CT scanner.

The aim of our study was to show by means of simulations that an attenuation-based current modulation system can in fact yield significant dose reduction without loss of image quality. Our particular approach in this investigation was to keep the total scan dose constant and to evaluate the resulting noise levels. Since noise variance and dose are inversely proportional, this allows a direct estimate of the possible dose reduction when constant noise is used as an endpoint.

In a second paper, a validation of the results of these simulations with physical phantoms will be presented.

II. THEORY

A. Basic principles

In general, the cross section of the human body differs significantly from a circular shape. Hence, for different CT view angles the x-ray pathlength and, therefore, the attenuation of the x-ray beam vary significantly. As a result, quantum noise also varies over a wide range often leading to very inhomogeneous pixel noise patterns in the final CT image. The basic idea is to homogenize noise by somehow adapting the x-ray intensities, i.e., tube current, to the projection-dependent attenuation. As an arbitrary model, consider the transmission of x-rays through the central pixel of a uniform,

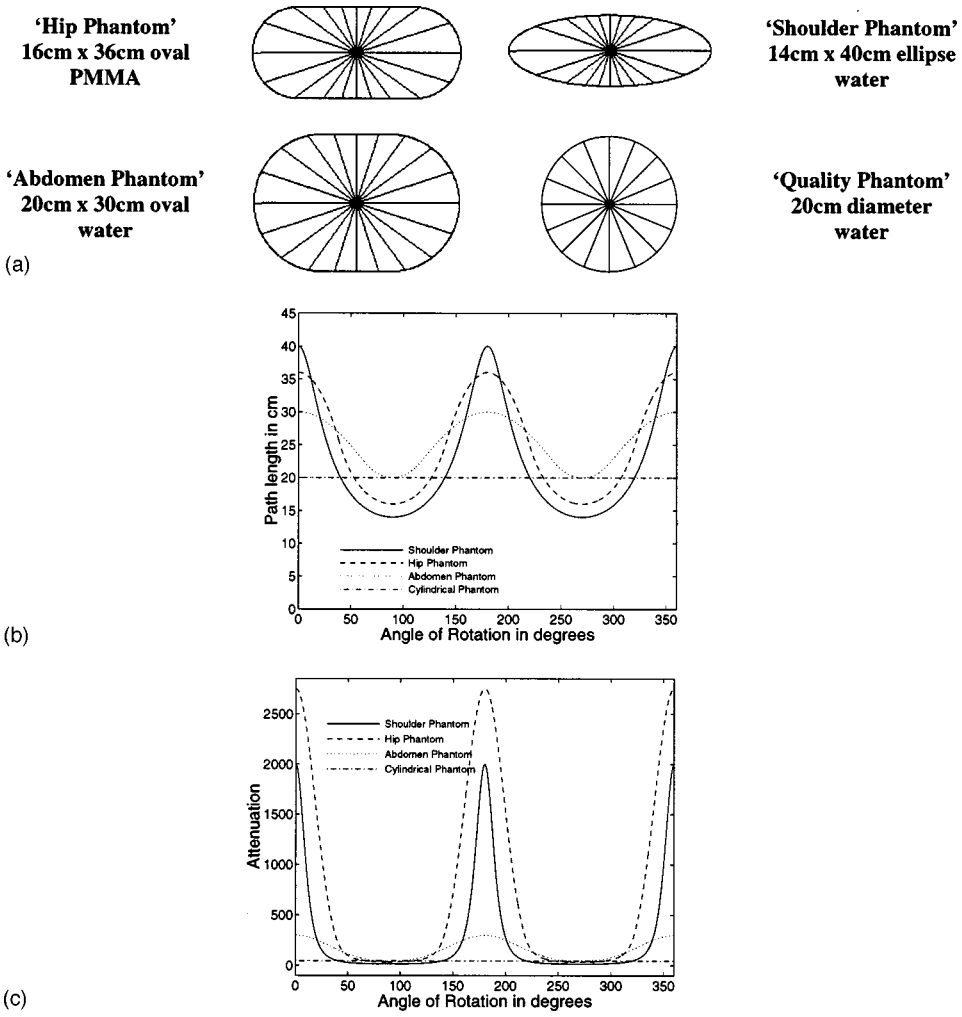

FIG. 1. Mathematical phantoms used in this study (a), related path lengths (b) and attenuation (c) for the central ray as a function of projection angle (see Sec. III B and Table I). While attenuation is constant and low for the 20 cm diameter cylindrical water phantom, it spans two orders of magnitude or more for the hip or shoulder geometry.

unity density elliptical object. The pathlength through the center of the ellipse as a function of view angle determines the resulting attenuation. This is illustrated in Fig. 1 for several standard objects. It is evident that pathlength and attenuation are constant for the central ray in a cylindrical object; it is worthwhile to note that attenuation can change by more than two orders of magnitude for objects approximating the shoulder or pelvic region (Table I).

The basic idea of a tube current modulation system can be explained by means of Fig. 2. The dotted lines show the case without tube current modulation. Primary radiation intensity is constant over all view angles (a), hence the transmitted (registered) intensity varies with attenuation (b). As a result, the noise level (variance) varies with view angle, i.e., inversely with the registered intensity (c). The solid lines show a control system, which modulates tube current as a function of attenuation such that the registered intensities are kept constant over all projections. In this case, tube current (a) has exactly the same angular dependence as the attenuation so that the registered intensities (b) and, therefore, data noise (c) are kept constant. This implies that intensity will be both decreased and increased as compared to the original setting. The dashed curves show the intermediate case of tube current adapted to the square root of attenuation. It will be shown that this moderate case of tube current modulation results in an optimum for pixel noise reduction.

To model the tube current modulation we define the modulation parameter α, which we vary between 0.0 and 1.0 such that 0.0 corresponds to the noncontrolled case and 1.0 to an adaptation proportional to attenuation. From a physical

TABLE I. Parameters for the four mathematic phantoms used in the simulations (compare Fig. 1).

Phantom	μ, cm^{-1}	d_{max}, cm	d_{min}, cm	A_{max}	A_{min}	H	H_{rel}
Shoulder phantom	0.19	40	14	1998	14	142	0.992
Hip phantom	0.22	36	16	2751	33	83	0.988
Abdomen phantom	0.19	30	20	299	45	7	0.849
Quality phantom	0.19	20	20	45	45	1	0.0

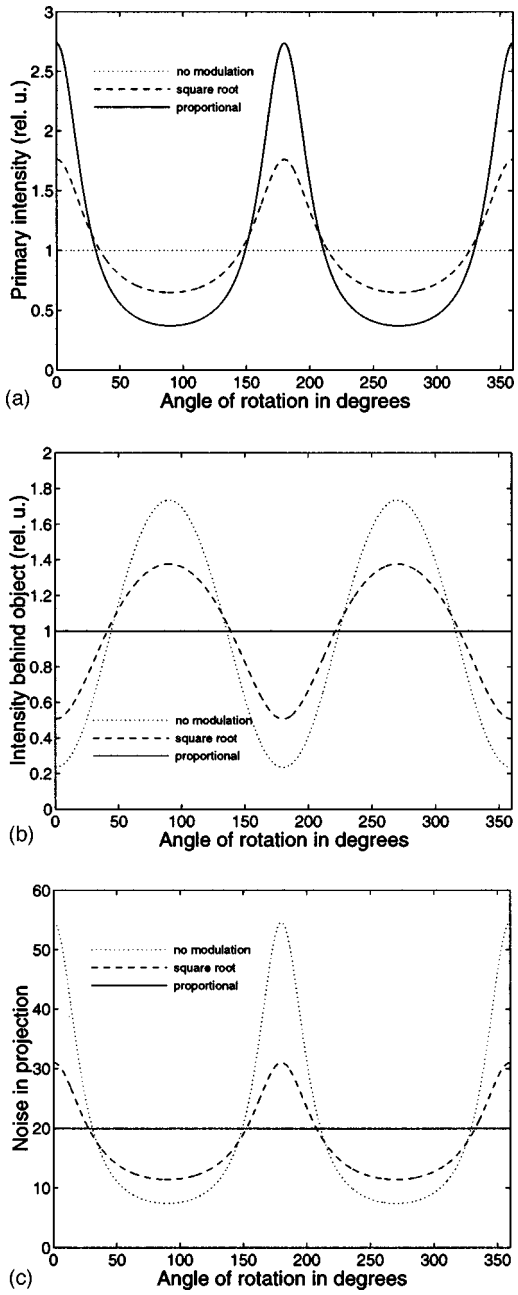

FIG. 2. Principle of tube current modulation. Primary intensities (a) have to be modulated as a function of attenuation in such a way that intensities behind the object (b) and the resulting noise (c) are either constant or distributed according to a predetermined function. Curves are shown for the elliptical shoulder phantom for constant current and for current modulation directly proportional to attenuation and proportional to the square root of attenuation.

point of view α is a scaling factor: Primary intensity is adapted proportional to attenuation, but for an object which is scaled by α. With attenuation being $A=e^{\mu\cdot L}$, the attenuation-based current modulation function is calculated according to $e^{\alpha\cdot\mu\cdot L}=A^{\alpha}$. As a special case, $\alpha=0.5$ corresponds to modulation by the square root of attenuation.

B. Analytical calculations

It can be shown that tube current control proportional to the square root of attenuation yields the optimal pixel noise level for given total dose. As a model, we consider pixel noise for the central pixel as a function of control strength. To simplify matters, we consider only the central rays passing through that pixel. This approximation corresponds to simple (nonfiltered) backprojection, which, though inappropriate for image reconstruction, provides a convenient estimate for pixel noise since variances are added directly. For the objects considered in our simulations as well as those encountered in clinical CT, the difference in attenuation between the central ray and its immediate neighbors is negligible. Thus, our simple model should provide meaningful results.

Let N_P be the number of views (projections), N_{0i} the emitted number of quanta for the central ray in view i and N_i accordingly the number of quanta in view i after traversing the object. The attenuation of the central ray in view i is then given by $A_i=N_{0i}/N_i$.

Pixel noise variance σ_P^2 for the central pixel is calculated as

$$\sigma_P^2=\sum_{i=1}^{N_P}\sigma_i^2=\sum_{i=1}^{N_P}\frac{A_i}{N_{0i}}. \tag{1}$$

Note that this expression gives pixel noise in the above-mentioned approximation as a function of control strength, since the latter determines the number of emitted quanta in each projection. It is subject to the boundary condition that the total number of emitted quanta per 360° scan $\Sigma_{i=1}^{N_P}N_{0i}=N_0$ is proportional to dose and is kept constant. Without this boundary condition our search for minimum noise would simply lead to the trivial result that we should use infinitely many quanta for each view, and noise would be zero.

As a result of the boundary condition given by the constant overall number of quanta, any one of the numbers N_{0i} may be expressed in terms of the remaining numbers. For example, $N_{01}=N_0-\Sigma_{i=2}^{N_P}N_{0i}$. The pixel noise variance becomes

$$\sigma_P^2=\frac{A_1}{N_0-\Sigma_{i=2}^{N_P}N_{0i}}+\sum_{i=2}^{N_P}\frac{A_i}{N_{0i}}. \tag{2}$$

The numbers of emitted quanta per view are now distributed in such a way as to minimize variance; this means that the partial derivative of the expression for variance with respect to each of the quantum numbers N_{0i} must be set to zero. The term being symmetric in its variables, it suffices to do this for any arbitrary view i, with $i\neq 1$. Thus, we get a relationship between number of quanta and attenuation for each view, which must be fulfilled for minimum pixel noise

$$\frac{\partial}{\partial N_{0i}}\sigma_P^2=(-1)\cdot\frac{-A_1}{(N_0-\Sigma_{i=2}^{N_P}N_{0i})^2}+\frac{-A_i}{N_{0i}^2}=0,$$

and consequently

$$\frac{A_1}{(N_0-\Sigma_{i=2}^{N_P}N_{0i})^2}=\frac{A_i}{N_{0i}^2}. \tag{3}$$

The denominator of the left hand side being N_{01}^2, we get the general relationship which holds for any view number i for the case of minimum noise at given total dose or number of quanta, respectively

$$\frac{A_i}{N_{0i}^2}=\frac{A_1}{N_{01}^2}=\text{const or } N_{0i}=\text{const}\cdot\sqrt{A_i}. \tag{4}$$

Thus, noise for the central pixel should be minimal for tube current modulated by the square root of the given angular-dependent attenuation, which means $\alpha=0.5$ according to our definition.

The constant in Eq. (4) is determined by the overall number of quanta resulting in

$$\sum_{i=1}^{N_P} N_{0i}=\sum_{i=1}^{N_P} \text{const}\cdot\sqrt{A_i}=N_0 \quad \text{or const}=\frac{N_0}{\Sigma_{i=1}^{N_P}\sqrt{A_i}}. \tag{5}$$

Therefore, the distribution of quanta for individual views should be controlled according to

$$N_{0i}=\frac{N_0}{\Sigma_{i=1}^{N_P}\sqrt{A_i}}\cdot\sqrt{A_i}, \tag{6}$$

to achieve minimum noise. The level of noise for this case is

$$\sigma_P^2=\sum_{i=1}^{N_P}\frac{A_i}{N_{0i}}=\sum_{i=1}^{N_P}\frac{A_i}{\left(\frac{N_0}{\Sigma_{k=1}^{N_P}\sqrt{A_k}}\right)\cdot\sqrt{A_i}}$$

$$=\frac{1}{N_0}\cdot\left(\sum_{i=1}^{N_P}\sqrt{A_i}\right)^2. \tag{7}$$

It can be derived analogously that the variance for any arbitrary value of control strength is

$$\sigma_P^2=\sum_{i=1}^{N_P}\frac{A_i}{N_{0i}}=\sum_{i=1}^{N_P}\frac{A_i}{\left(\frac{N_0}{\Sigma_{k=1}^{N_P}\sqrt{A_k^\alpha}}\right)\cdot A_i^\alpha}$$

$$=\frac{1}{N_0}\left(\sum_{i=1}^{N_P}A_i^{1-\alpha}\right)\cdot\left(\sum_{i=1}^{N_P}A_i^\alpha\right). \tag{8}$$

This expression leads to the remarkable result that noise is the same for the cases of $\alpha=0$ (no control at all) and $\alpha=1$ (control proportional to attenuation).

$$\sigma_P^2=\sum_{i=1}^{N_P}\frac{A_i}{N_{0i}}=\frac{1}{N_0}\left(\sum_{i=1}^{N_P}A_i^1\right)\cdot\left(\sum_{i=1}^{N_P}A_i^0\right)$$

$$=\frac{1}{N_0}\left(\sum_{i=1}^{N_p}A_i\right)\cdot\left(\sum_{i=1}^{N_p}1\right)=\frac{N_P}{N_0}\sum_{i=1}^{N_p}A_i. \tag{9}$$

This can be understood intuitively if one takes into account that the total number of quanta per scan is limited. To invest in the high-attenuation projections to obtain equal detected numbers for all projections would lead to higher noise contributions from low-attenaution projections. Noise would be more homogeneous and unstructured, but many more of the primary quanta would be absorbed in the object resulting in higher image noise levels.

III. MATERIALS AND METHODS

A. General

We performed simulations to answer a variety of questions about the effect of tube current control on pixel noise reduction. All calculations were performed for four simple phantoms [Fig. 1(a)] for which we have physical counterparts. The results from the physical phantoms will be presented and discussed in a subsequent paper (part II).

First, noise in the central pixel of different phantoms was calculated in the central-beam approximation. This model allows for the quantification of possible noise reduction and the efficiency of tube current modulation for a variety of phantoms as well as the dependence on several parameters.

Second, the effect of tube current modulation on the reconstructed images was evaluated by simulating the transmission projections for each of the phantoms. The projections were scaled proportional to the expected tube current and noise was added.

All simulations were carried out for a constant attenuation coefficient μ for a typical 120 kVp spectrum. The dose per view was defined as the number of quanta N_{0i} emitted by the tube. The number N_i was calculated for the traversed path length L_i as $N_{0i}e^{-\mu\cdot L_i}$. Finally, data noise was calculated from the number of registered quanta. Noise amplitudes are given in terms of the variance σ^2. As noted in the introduction, this allows a direct quantification of the possible dose reduction when constant noise is used as an endpoint.

Although we used realistic numbers of quanta per ray (10^7), the results of our simulations do not depend on that assumption. This is because we evaluated the relative degree of noise reduction, which is independent of the number of quanta.

For most of the simulations, both a sinusoidal and an attenuation-based modulation function with varied control parameter α were used.

B. Simulation of noise levels in central ray approximation

As pointed out above, the central ray approximation provides an acceptable model for calculating the image noise of the central pixel.

We used the following elliptical and oval shapes as the simulation objects:

1. An elliptical ''shoulder phantom,'' 40 cm by 14 cm size, attenuation $0.19\,\text{cm}^{-1}$ (''water'');

2. an oval ''hip phantom,'' 36 cm by 16 cm size, attenuation $0.21\,\text{cm}^{-1}$ (''acrylic'');

3. an oval ''abdomen phantom,'' 30 cm by 20 cm size, attenuation $0.19\,\text{cm}^{-1}$ (water);

4. a circular phantom, 20 cm diameter, attenuation $0.19\,\text{cm}^{-1}$ (water).

The shapes of these phantoms together with their angle-dependent radius and the corresponding attenuation are shown in Fig. 1.

The simulations were carried out as follows:

1. Calculation of attenuation-weighted path length $\mu \cdot L(\varphi)$.

The length $L(\varphi)$ of the intersection of the virtual x-ray with the object is calculated from its polar representation.

For an elliptical shape with half axes a and b, this is

$$r(\varphi)=\frac{b}{\sqrt{1-\varepsilon^2\cos^2}}, \tag{10}$$

where $\varepsilon=\sqrt{a^2-b^2}/a$.

For an oval shape with the same half axes ($e=a-b$ denotes their difference), we get

$$r(\varphi)=\begin{cases}\sqrt{2e|\cos\varphi|\sqrt{b^2-e^2\sin^2\varphi}+2e^2\cos^2\varphi+b^2-e^2}, & \text{if } |\tan\varphi|<b/e\\ \dfrac{b}{|\sin\varphi|}, & \text{if } |\tan\varphi|\geqslant b/e\ .\end{cases} \tag{11}$$

Of course, the length of a diameter d through the center is twice the radius r given in the polar representation: $L(\varphi)=d(\varphi)=2r(\varphi)$. The attenuation weighted path length which the x-ray traverses is then $\mu \cdot d(\varphi)$.

2. Calculation of attenuation of the central ray $A(\varphi)=e^{\mu \cdot d(\varphi)}$.

3. Calculation of a current modulation function $w(\varphi)$.

The number $N_0(\varphi_i)=N_{0i}\cdot w(\varphi)$ of emitted quanta for each view is determined according to the angle-dependent attenuation with respect to the desired control strength and modulation function.

In the case of the fixed shape function, only the minimum and maximum attenuation values are used to calculate a sinusoidal modulation function for tube current. If $A_{\min}$ and $A_{\max}$ denote minimum and maximum attenuation during one tube rotation, the modulation function becomes

$$w(\varphi)=A_{\min}+\frac{A_{\max}-A_{\min}}{2}(1+\cos 2\varphi). \tag{12}$$

To simulate the control strength α, $A_{\min}^{\alpha}$ and $A_{\max}^{\alpha}$ are used instead of $A_{\min}$ and $A_{\max}$.

The attenuation-based modulation function is directly adapted from the attenuation values and the desired control strength

$$w(\varphi)=A(\varphi)^{\alpha}. \tag{13}$$

These weight functions are normalized to the constant overall number of quanta N_0 which has to be distributed over all projections.

4. Calculation of pixel noise for the modulation function under consideration.

The number of registered quanta follows from the division of the emitted number of quanta at a specified projection by the corresponding attenuation:

$$N(\varphi)=\frac{N_0(\varphi)}{A(\varphi)}=N_0(\varphi)\cdot e^{-\mu \cdot d(\varphi)}. \tag{14}$$

The noise variance associated with the central ray for this projection angle $\sigma_M^2(\varphi)$ is inversely proportional to the number of measured quanta

$$\sigma_M^2(\varphi)=\frac{1}{N(\varphi)}. \tag{15}$$

Pixel noise depends on the individual projection variances and is calculated as

$$\sigma=\frac{1}{N_0}\sqrt{\sum_i \sigma_M^2(\varphi_i)}. \tag{16}$$

C. Simulation of CT images with noise

It is important not only to examine the effect of tube current modulation on noise levels, but also on the distribution and structure of noise in actual images. To accomplish this, we calculated sinogram data using parallel geometry for simple elliptic and circular objects. Noise was added as described below, and images were reconstructed using filtered backprojection with a Shepp–Logan convolution kernel.

To calculate the sinogram data, again the attenuation-weighted pathlength $L(\varphi,p)$ of a ray with projection angle φ and distance p to the origin through the object is determined.

For a centered ellipse with half axes a and b, we get

$$L(\varphi,p)=2ab\frac{\sqrt{(a^2\cos^2\varphi+b^2\sin^2\varphi)-p^2}}{a^2\cos^2\varphi+b^2\sin^2\varphi}. \tag{17}$$

Similarly, for a circular cross-section with center (x,y) and radius r we get

$$L(\varphi,p)=2\sqrt{r^2-(p-x\cos\varphi-y\sin\varphi)^2}. \tag{18}$$

These expressions become purely imaginary when there is no intersection. As we consider the real part only, no distinction is necessary.

We simulated an ellipse (shoulder phantom) with and without an additional matrix of 16 circular low-contrast holes (diameter 1 cm, 1 cm separation, $\Delta\mu=0.002\,\mathrm{cm}^{-1}$, according to a contrast of 1%).

The ideal measurement without noise correspondents to the sum of all path lengths through the object, weighted with the appropriate attenuation coefficient μ

$$f_{lk}^{0} = \sum_{\text{Object } i} \mu_i \cdot L_i(\varphi_l, p_k). \tag{19}$$

Noise is added to each value f_{lk}^{0} by scaling normalized random numbers $\zeta(0,1)$, i.e., with mean 0, standard deviation 1 and Gaussian distribution, with the standard deviation $\sigma = 1/\sqrt{N_{lk}}$. The number of registered quanta N_{lk} in projection l and channel k is calculated as A_{lk}.

Thus, the noise affected data become

$$f_{lk} = \sum_{\text{Object } i} \mu_i \cdot L_i(\varphi_l, p_k) + \sqrt{\frac{A_{lk}}{N_l}} \cdot \zeta_{lk}(0,1). \tag{20}$$

The data set obtained in this manner has the correct data noise with respect to both attenuation and tube current modulation. It is reconstructed using a Shepp–Logan convolution kernel as a pixel matrix in the usual manner. The choice of kernel will influence the absolute noise levels, but it does not influence the relative changes reported below.

The structure and level of the pixel noise will vary for each realization if the random number set that generates the data noise is allowed to change. We observed typical variations in the σ estimates of 10% for different sets of random numbers. These variations will be combined with the effect of tube current modulation. Therefore, to monitor the effect of dose control only without being affected by different random noise samples, we have used the same set of random numbers to generate the noise for each simulation. Thus, we can evaluate the pixel noise dependence with respect to control strength with single simulations instead of determining the statistical properties of many independent images.

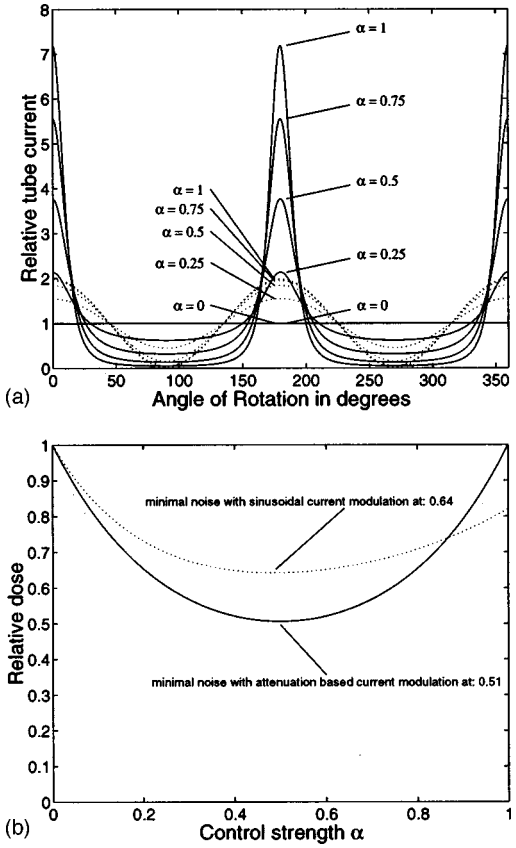

FIG. 3. Dependence of noise reduction on the tube current modulation control strength α for the shoulder phantom. (a) Modulation functions for different control strength vary from constant to a shape, which corresponds to the attenuation function for the central ray, plotted against rotation angle. Solid lines are shaped according to actual attenuation, while dotted lines are sinusoidal. (b) Each modulation curve in (a) results in a specific overall noise reduction. Noise reduction plotted against control strength α shows a parabolic shape when modulation is varied according to actual attenuation. For control strength 0.5, pixel noise is minimized. The noise reduction is much less if a sinusoidal shape is used for the modulation function (dotted line).

IV. RESULTS AND DISCUSSION

A. Noise level calculations

In the following sub-sections, the results of image noise calculations using the central ray approximation are presented. Unless otherwise mentioned, the object studied is always the shoulder phantom.

1. Noise reduction as a function of current control strength α

If control strength α is varied continually between zero and one for a specific object, the modulation functions are distorted continually from a constant tube current to the maximum adaptation directly proportional to attenuation [set of solid curves in Fig. 3(a)]. The dotted curves are sinusoids with the same amplitude. The integral of all these functions is kept constant, corresponding to a constant total scan dose.

Every value of α corresponds to a different modulation function and, hence, to a different noise amplitude. Plotting pixel variance against α, we get a parabolic curve if the modulation function is shaped by the actual attenuation values [Fig. 3(b)]. We rediscover our theoretical predictions that noise is at a minimum for $\alpha = 0.5$ and that it has the same value for both the noncontrolled ($\alpha = 0$) and the maximally adapted case ($\alpha = 1$), where noise is equal for all central rays.

If a sinusoidal modulation function is used (dotted curve), noise reduction is much less and the dependence on control strength is no longer symmetric.

That is, online attenuation-based current modulation is superior to using sinusoidal modulation functions which are not sensitive to object shape.

2. Noise reduction as a function of object shape and size

The dependence of noise reduction on the shape and size of the object is complicated and does not lend itself to simple answers. Yet some insight can be gained from the simulations to help estimate the effect of tube current modulation.

It is clear that attenuation-based modulation of tube current cannot have any noise reduction effect for a circular object and that increasing benefit is to be expected for increasing deviation from circular symmetry. The relative

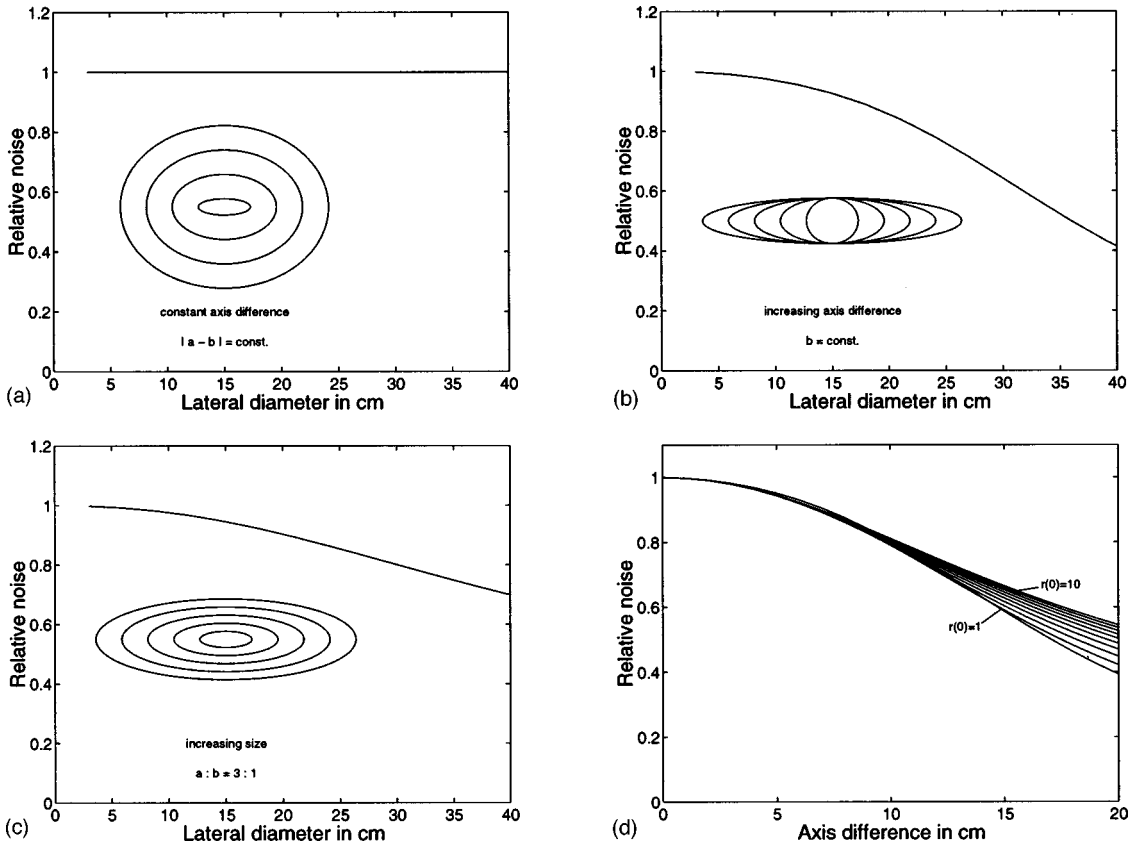

FIG. 4. Dependence of noise reduction on object shape and size. (a) Shapes of ellipses with constant axis difference, starting with 2 cm by 6 cm and increasing by 1 cm in each direction. The object shape approaches a circular form. Noise reduction by tube current control is constant for objects with the same difference between long and short axes. (b) Shapes of ellipses with increasing axis difference, starting with 1:1 and increasing to 1:15. For objects with increasing axis difference (b), we get a rapidly increasing efficiency of noise reduction by dose control. (c) Shapes of ellipses with increasing size; long half axes are the same as in (b). For objects with increasing size, the corresponding noise reduction has a similar, but smaller dependence on the size of the long half axis, because the shapes differ less from a circular one. Noise reduction also depends in a similar manner on attenuation coefficient as on size. For the central beam, the effect is the same. (d) The amount of noise reduction depends more on axis difference than on size or shape of the objects. Curves have axis difference grow in the same manner as indicated on the abscissa, but the lower one starts with a circle of radius 1 cm, the upper with radius 10 cm, so the variation in shapes is different.

noise reduction depends only on the shape and not on the absolute value of the attenuation function. The relative amplitude H of the attenuation function is the relation of the maximum attenuation $A_{\max}$ to the minimum attenuation $A_{\min}$. This ratio in turn depends on the difference $(d_{\max} - d_{\min})$ between the long diameter $d_{\max}$ and short diameter $d_{\min}$, and the attenuation coefficient μ

$$H = \frac{A_{\max}}{A_{\min}} = \frac{e^{\mu d_{\min}}}{e^{\mu d_{\max}}} = e^{\mu(d_{\max} - d_{\min})}. \tag{21}$$

The amplitude of the modulation function is determined by Eq. (21). Therefore, the axis difference $d_{\max} - d_{\min}$ and attenuation coefficient μ are reasonable parameters to examine in our investigation of noise reduction.

It follows that objects with the same attenuation coefficient and the same path length difference between their half axes should display similar behavior with respect to noise reduction. Indeed, ellipses of the series 1:3, 2:4, 3:5, 4:6, ... show almost exactly the same behavior even though their shapes become more and more circular [Fig. 4(a)]. Noise reduction remains the same.

The potential for noise reduction increases strongly with axis difference. The shapes of respective objects are shown in Fig. 4(b) and vary from 1:1 up to 1:15.

Figure 4(c) shows the dependence of noise reduction with respect to object size (or equivalently, attenuation coefficient). The ellipses in this object set maintain a 1:3 axis ratio with the long half axis varied from 3 to 20 cm. It is obvious that noise reduction behavior is similar to that observed for the case of increasing axis difference, although the magnitude is smaller. This is understandable since this set of ellipses is closer to a circular shape and the axis difference increases comparatively slowly.

The dependence of noise reduction on shape is comparatively small again. The set of curves in Fig. 4(d) shows noise reduction as a function of axis difference. For these objects, the short half axis is held constant while the long half axis is increased by 0–10 cm over the value of the short half axis. Sets of 10 objects were included with the short half axis ranging from 1 to 10 cm. Thus, the first object (bottom curve) starts as a circle of radius 1 cm and is distorted to a 1:11 ellipse, while the largest object (top curve) is distorted

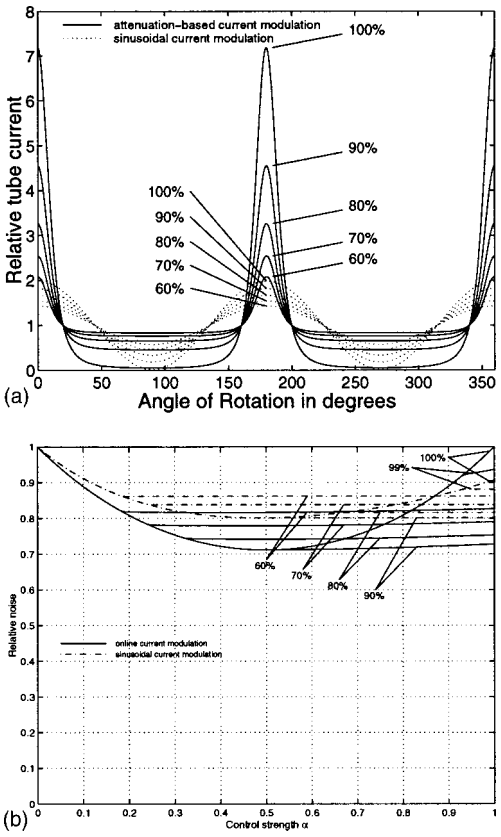

FIG. 5. Dependence of noise reduction on amplitude limitation of tube current modulation. (a) Modulation curves for the same elliptic object (shoulder phantom), with different limitations in amplitude. The curve with highest amplitude (100% modulation) corresponds to attenuation. Dotted lines are sinusoidal modulation curves with the same amplitudes. (b) Effect of limited modulation amplitude on noise reduction: Once the limitation is reached, no further noise reduction is achieved. The curves leave the ideal parabolic track and remain almost constant.

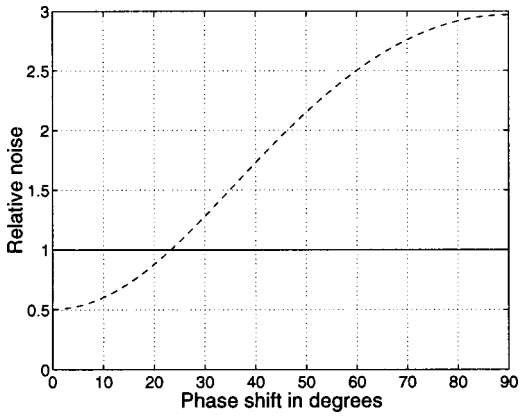

FIG. 6. Dependence of noise reduction on phase shifts between attenuation function and modulation function. The noise levels increase slowly at first indicating that a small lag in tube current response may not be critical. For large phase shifts, however, current modulation control becomes counterproductive, noise exceeds far that obtained with constant current.

to a 10:20 ellipse. When one considers the substantial range of object shapes in this simulation, the small effect on noise reduction as function of axis difference is remarkable.

A further understandable finding is that ellipses with the same ratio between long and short half axes, hence the same shape but different size, show the same behavior with respect to noise reduction as do ellipses of identical outline but with different attenuation coefficients μ. In the central ray approximation, these two cases are identical since for the central ray it does not matter whether different attenuation stems from a longer path or from a more strongly absorbing material.

3. Noise reduction as a function of limited modulation amplitude

Arbitrary modulation of the tube current as a function of time is difficult because of the system operating limits. In practice, current modulation is often implemented by simply clipping the current modulation function at limiting values; a more sophisticated approach is to scale and fit the given curve shape between the limits.

In our simulation, the limiting amplitude (i.e., the lowest current value) is given as a percentage of the maximum current value. Because the total scan dose is kept constant, the maximum projection intensity is automatically increased if dose is lowered over other projections. A limiting amplitude of 90% means that the dose modulation function may vary between 10% and 100% of the maximum current value.

If $A_{\min}$ and $A_{\max}$ again denote the minimum and maximum attenuation and hence the minimum and maximum of an ideal modulation function, then the (relative) amplitude for modulation according to attenuation with control strength α is given as

$$H_{\text{rel}}=\frac{A_{\max}^{\alpha}-A_{\min}^{\alpha}}{A_{\max}^{\alpha}}=1-H^{-\alpha}. \tag{22}$$

If the limiting amplitude has a value of $H_{\lim}$ (given as a fraction of one), then a modulation function with the same shape but respecting the given limits is given by

$$\bar{w}(\varphi)=\begin{cases}\dfrac{H_{\lim}A_{\max}^{\alpha}}{A_{\max}^{\alpha}-A_{\min}^{\alpha}}\cdot(w(\varphi)-A_{\max}^{\alpha})+A_{\max}^{\alpha} & \text{if } H>H_{\lim}\\ w(\varphi) \quad \text{if } H\leqslant H_{\lim}.\end{cases} \tag{23}$$

Assuming limiting amplitudes of 100%, 99%, 90%, 80%, 70%, and 60%, noise reduction, was calculated for these limited modulation functions against control strength. Results are plotted in Fig. 5.

The set of curves in Fig. 5(a) shows modulation functions with different limiting amplitudes for maximum control strength (directly proportional to attenuation). In comparison with Fig. 3(a), the modulation function curves with maximum control strength ($\alpha=1$) which have been restricted by the limiting amplitude are very similar to curves with reduced control strength.

The set of curves in Fig. 5(b) shows noise reduction plotted as a function of control strength for five different limiting amplitudes. It is clear that once the limiting amplitude be-

TABLE II. Simulated dose reduction for three phantoms and a typical patient dataset. Left column (Limit): Amplitude limitation of modulation. Second column (Min): Minimum achievable noise relative to the noncontrolled case for the given amplitude limitation. Third column (Sqrt): Relative noise when modulating proportional to the square root of attenuation. If no amplitude limitation is imposed, this is the optimal case. Last column (Prop): Relative noise when modulating proportional to attenuation. Without amplitude limitation the value is always one because noise is the same as in the noncontrolled case. (a)–(c) Data for the investigated phantoms. (d) Simulated dose modulation for a typical patient data set (shoulder region).

Limit	Min	Sqrt	Prop	Limit	Min	Sqrt	Prop
	(a) Shoulder phantom: Ellipse 40 cm×14 cm water ($\mu=0.19\ cm^{-1}$)				(c) Abdomen phantom: Oval 30 cm×20 cm: ($\mu=0.19\ cm^{-1}$)		
	Attenuation based				Attenuation based		
100%	0.5062	0.5062	1.0000	100%	0.9053	0.9053	1.0000
90%	0.5076	0.5076	0.5298	90%	0.9053	0.9053	1.0000
80%	0.5496	0.5496	0.5675	80%	0.9053	0.9053	0.9531
70%	0.6070	0.6071	0.6245	70%	0.9053	0.9053	0.9145
60%	0.6663	0.6668	0.6834	60%	0.9054	0.9054	0.9065
	Sinusoidal				Sinusoidal		
100%	0.6423	0.6424	0.8228	100%	0.9055	0.9055	0.9739
90%	0.6426	0.6426	0.6426	90%	0.9055	0.9055	0.9739
80%	0.6662	0.6662	0.6662	80%	0.9055	0.9055	0.9383
70%	0.7027	0.7027	0.7027	70%	0.9055	0.9055	0.9099
60%	0.7430	0.7430	0.7430	60%	0.9058	0.9058	0.9058
	(b) Hip phantom: Oval 36 cm×16 cm acrylic ($\mu=0.21\ cm^{-1}$)				(d) Patient data (central ray)		
	Attenuation based				Attenuation based		
100%	0.6139	0.6139	1.0000	100%	0.5381	0.5381	1.0000
90%	0.6139	0.6139	0.6350	90%	0.5470	0.5473	0.5689
80%	0.6330	0.6334	0.6421	80%	0.5957	0.5960	0.6133
70%	0.6733	0.6739	0.6799	70%	0.6517	0.6518	0.6701
60%	0.7193	0.7197	0.7249	60%	0.7072	0.7073	0.7260
	Sinusoidal				Sinusoidal		
100%	0.6676	0.6691	0.7676	100%	0.6364	0.6366	0.6913
90%	0.6680	0.6691	0.6680	90%	0.6409	0.6409	0.6409
80%	0.6910	0.6910	0.6910	80%	0.6719	0.6719	0.6719
70%	0.7256	0.7256	0.7256	70%	0.7103	0.7103	0.7103
60%	0.7636	0.7636	0.7636	60%	0.7510	0.7510	0.7510

comes a factor, increasing control strength yields no significant further benefits. Image noise is essentially constant when control strength exceeds 0.5. It is remarkable that even for very small limits in amplitude (99% for our shoulder phantom) the noise symmetry that was previously found to exist for control strength zero and one is destroyed. For limited modulation amplitude an asymmetry will always remain when α approaches 1.

However, the result is not surprising if we keep in mind that the shape of the modulation function can not vary much once the limiting amplitude has been reached. As a result, the choice of control strength $\alpha \geqslant 0.5$ has little influence when amplitudes larger than the limiting amplitude would be required.

4. Noise reduction as a function of modulation phase shift

Response times of tube current and emitted intensities may lead to a time lag or phase shift between the estimated-modulation function and the real response. The magnitude of this effect was evaluated by examining the behavior of noise by incrementally increasing the phase shift of the modulation function from 0 to 90 degrees. Simulations were performed for the shoulder phantom using an optimum modulation function (control strength 0.5). Results of this experiment are shown in Fig. 6. Phase shifts of less than five degrees appear to have minimal effect on the noise level. On the other hand, a phase shift of 25 degrees completely eliminates the desired effect of dose reduction. If the phase shift increases further, noise is raised far above its level without current control. This is easily understood since more dose is delivered to projections with low attenuation while dose is reduced for projections with high attenuation.

5. Achievable noise or dose reduction for different phantom shapes

The potential for noise reduction by current control was calculated as a function of both control strength and amplitude limitation for the elliptical shoulder phantom, the oval hip phantom and the oval abdomen phantom (Fig. 1). As previously pointed out, noise reduction (expressed as variance of pixel noise) is equivalent to the amount that the total scan dose could be reduced without losing image quality. Figure 7 shows the achievable noise and the respective dose reduction for both attenuation-based (solid) and sinusoidal (dotted) modulation functions as a function of control

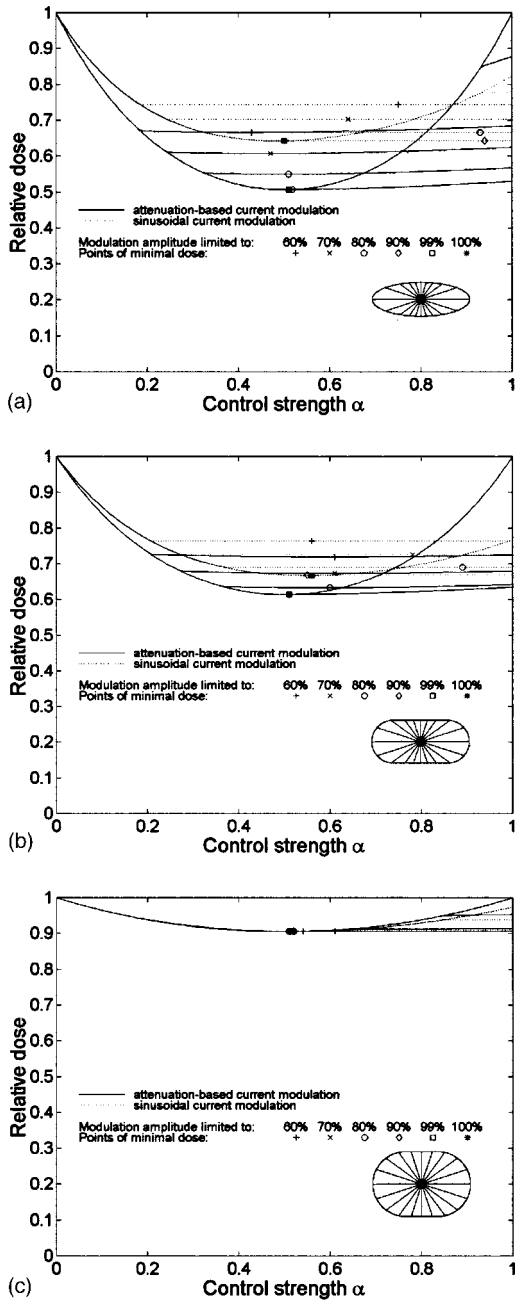

FIG. 7. Results of the efficiency of dose control for different phantoms. Noise reduction is plotted against control strength. Solid curves display results for dose control according to attenuation, dotted lines correspond to sinusoidal control functions with amplitude adapted to minimum and maximum attenuation. Each curve corresponds to a different amplitude limit (100%, 99%, 90%, 80%, 70%, 60%). (a) The shoulder phantom provides potential for dose reduction of up to 50% with attenuation based control functions, but only 35% for sinusoidal curves. (b) The hip phantom has less variation in path length due to its oval shape and thus yields less noise reduction. Also, the relative difference between attenuation-based and sinusoidal control functions is smaller. (c) The abdomen phantom is close to a circular shape and so has little potential for noise reduction. Noise levels can be reduced by about 10%, and there is almost no performance difference between attenuation based and sinusoidal modulation functions.

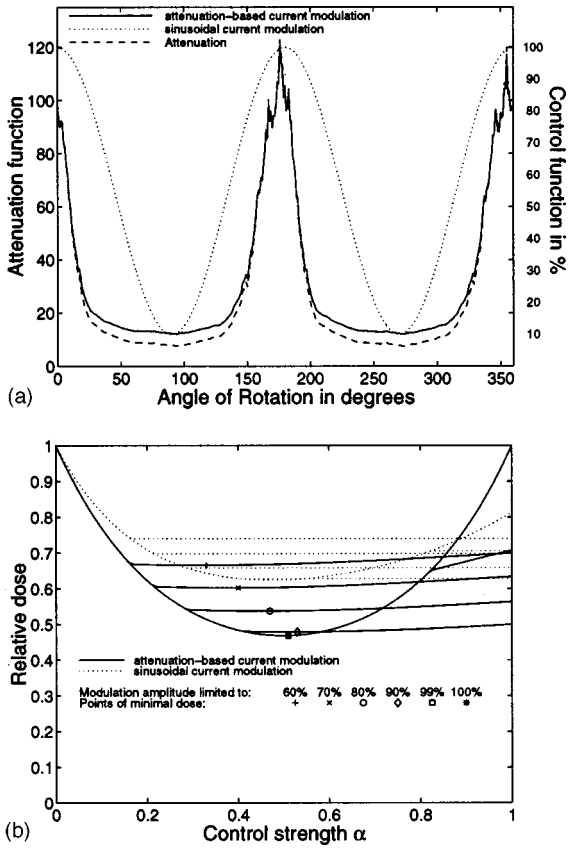

FIG. 8. Evaluation of patient data (shoulder scan). (a) Modulation function resulting from the angle-dependent attenuation for the central ray with $\alpha = 0.5$. The sinusoidal modulation function is not a good approximation. (b) The achievable noise reduction in this patient study corresponds well to the shoulder phantom simulation.

strength. Simulation of amplitude limitation was included. Curves are plotted for values of noise reduction with 100%, 99%, 90%, 80%, 70%, and 60% limiting amplitude. These curves show similar results as Fig. 5. Although the unlimited amplitude (100%) shows a symmetric parabolic shape, even small amplitude limits exhibit noticeable asymmetries by these plots.

In addition, real data from a patient study were evaluated (Fig. 8), and similar results were found. The central ray of a shoulder scan was treated in exactly the same way as for the simulated data. Figure 8(a) shows the modulation function governed by the square root of attenuation for the central ray (left scale) and the same shape rescaled and limited to 90% amplitude (right scale) as modulation function, together with the sinusoidal modulation function with the same amplitude. Figure 8(b) shows the achievable noise reduction for each of the modulation functions.

Numerical values of noise reduction are given in Table II for both attenuation-based and sinusoidal modulation functions for different values of limited amplitude. This includes noise reduction for maximum control strength ($\alpha = 1$), for optimum control strength ($\alpha = 0.5$) and the noise minimum which, if a limited amplitude is introduced, is no longer (in general) found at $\alpha = 0.5$.

Noise reduction was about 50% for the shoulder phantom, while the hip phantom had about 40%. A 10% noise reduction only was found for the abdomen phantom. This is expected because of the high eccentricity of the shoulder phantom and the low eccentricity of the abdomen phantom. The

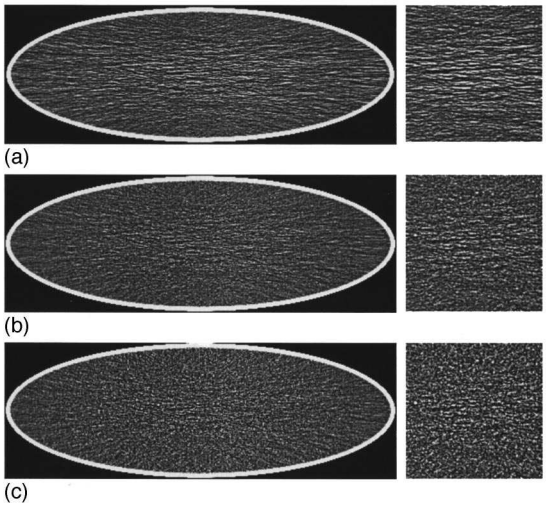

FIG. 9. Simulated images of an ellipse with noisy data. (a) With constant current ($\alpha=0.0$, SD=16.3 HU). Noise structure is streaky from left to right in the direction of maximum attenuation. (b) Current control with intermediate control strength ($\alpha=0.5$) produces minimal pixel noise levels (11.1 HU). (c) Current control with maximum control strength ($\alpha=1.0$) produces isotropic pixel noise levels (15.5 HU).

patient scan data which were acquired in the shoulder region show a very good correspondence with the shoulder phantom.

B. Image simulations

1. Homogenization of pixel noise by current control

Without tube current modulation, projections with high attenuation show a considerably higher noise level than those with low attenuation which results in a structured, anisotropic noise pattern extending in the direction of highest attenuation [Fig. 9(a)]. Noise is minimized for modulation according to the square root of attenuation ($\alpha=0.5$), noise amplitude is minimized, but with noise structure persisting.

If tube current modulation with maximum control strength is employed, the level of data noise is similar for all projections for the central channels. As a result, the pixel noise structure becomes isotropic [Fig. 9(c)].

2. Image noise as a function of control strength

Figures 10–12 show a mosaic of 12 images with the same field size of 10 cm by 10 cm in the center of the simulated shoulder phantom. Control strength is varied from 0.0 to 1.0 in steps of 0.1 spanning the range from the constant current case to maximum control. In order to fill the matrix and also to have a direct comparison between the extreme cases, the constant current case is repeated in the last partial image.

Figure 10(a) shows a simulation without amplitude limitation.

The variation of the noise patterns is exclusively due to the effect of current control since the same set of random numbers was used to calculate the data noise. The curve in

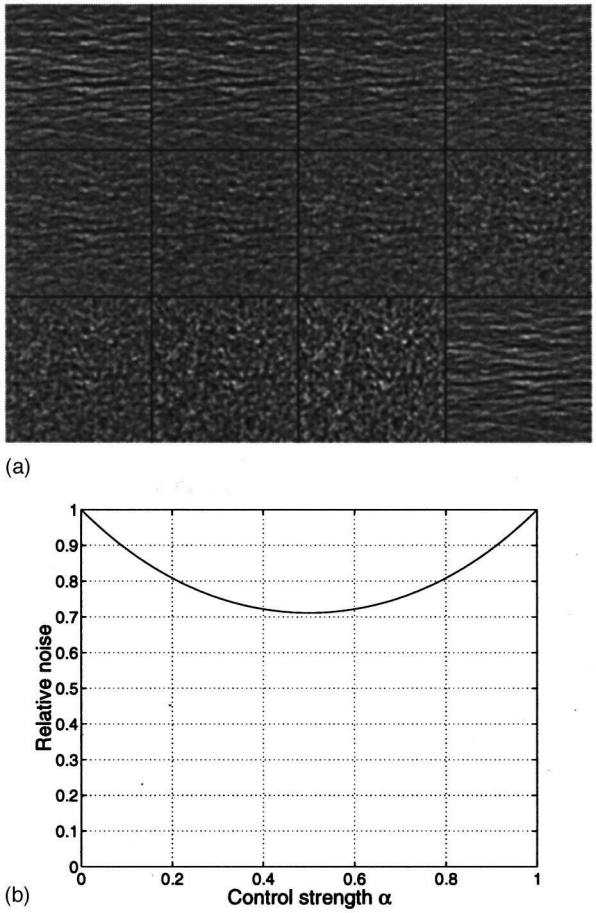

FIG. 10. Dependence of pixel noise on control strength. The mosaics consist of 12 partial images (a) each showing a 10 cm by 10 cm area inside the elliptic shoulder phantom. Control strength α varies as:

0.0	0.1	0.2	0.3
0.4	0.5	0.6	0.7
0.8	0.9	1.0	0.0

The plot of pixel noise for each partial images, taken directly as variance of the pixel values, shows the same dependence on control strength as in the preceding simulations (b).

Fig. 10(b) shows the expected parabolic behavior. Note that the maximally achieved noise reduction is less for this extended area than for the central pixel. The maximum of local noise in each partial image is in its center.

Two effects associated with increasing control strength are evident:

1. The structure of noise changes continually from an anisotropic to an isotropic pattern.

2. The amplitude of noise decreases until control strength has reached the value of 0.5 (proportional to square root of attenuation), then it increases again.

Figure 11 shows the same simulation as in Fig. 10, but with a limitation of amplitude to 90%. It becomes apparent that almost no more change occurs once the amplitude of the modulation function has reached its limit.

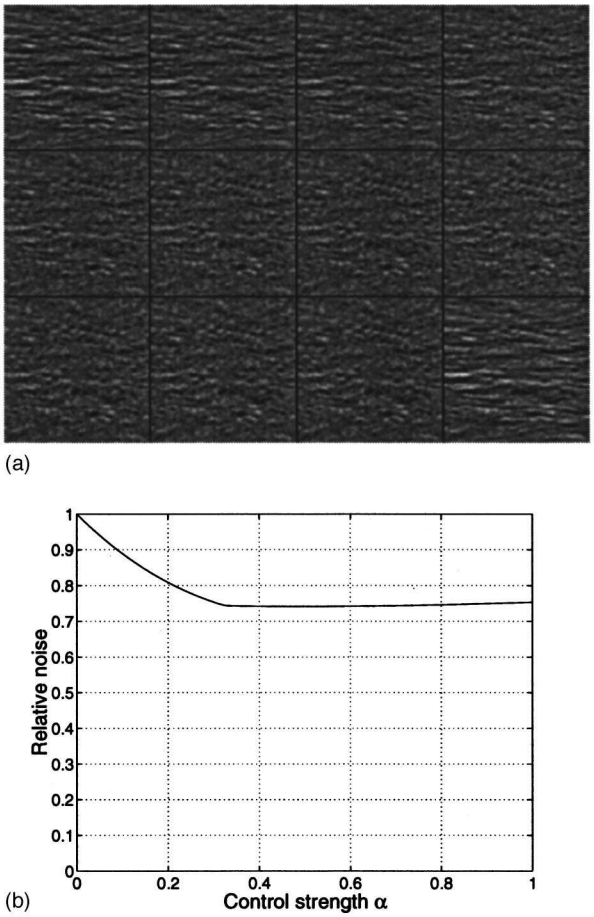

FIG. 11. Dependence of pixel noise on control strength and amplitude limit. (a) The same composite image as in Fig. 10, but calculated for an amplitude limitation of 90%. Once the amplitude limit has been reached, practically no further change in noise level is observed. (b) Pixel noise as function of control strength under limited amplitude; the behavior is much the same as in the central beam simulation.

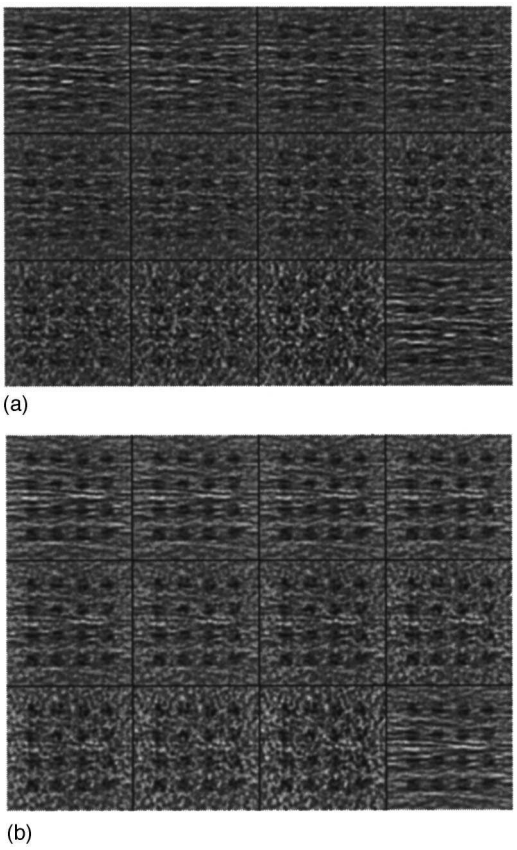

FIG. 12. Influence of dose control on low contrast detectability (composite images with control strength α varied as in Fig. 10). (a) An array of 16 holes with low contrast (10 HU) has been placed in the same area of the ellipse. Noise is lowest in the sixth partial image ($\alpha=0.5$) and visibility is best there. (b) Pixel noise has been kept constant for all partial images. The potential of current control to reduce noise was balanced by applying accordingly less dose. On all partial images, visibility is about the same, though about 30% less dose was used in the sixth image as compared to the first one. The relative dose used for each partial image is as follows:

1	0.89	0.8	0.73
0.69	0.68	0.68	0.70
0.76	0.85	0.98	1

3. Low contrast detectability as a function of tube current modulation

In the next simulation, the same area of the shoulder phantom is simulated and reconstructed with an additional matrix of 16 holes with 1 cm diameter, 2 cm center-to-center distance and a contrast of 10 HU. The partial images are composed as described above.

Figure 12(a) shows a simulation with increasing control strength and constant overall dose, as in the preceding simulations. Since the minimum noise level is found for $\alpha=0.5$, the holes are best perceived in the sixth partial image (i.e., second row, second column). Though nominal noise is the same for partial images 1 ($\alpha=0$) and 11 ($\alpha=1$), the holes are less visible in the latter due to the different noise structure. This holds for this size of holes and noise pattern, it is not a general result; on the contrary a homogeneous, isotropic noise pattern is generally considered superior both aesthetically and diagnostically. The example shows, however, that nominal noise amplitude is only one parameter among many for judging image quality.

Instead of utilizing current control to improve image quality for a constant total scan dose, one can also achieve dose reduction while maintaining image quality. Because of the relationship between dose and pixel noise, the overall dose can be lowered by an amount compensating for the gain in noise reduction. This is illustrated in Fig. 12(b) where the noise is the same for all partial images, but simulated dose was reduced 2%. In fact, the visibility of the pattern is about the same for all partial images.

C. Understanding noise reduction by means of tube current modulation

Tube current modulation redistributes the total exposure unequally over all projections. In the central ray approximation, the contribution of every projection to image noise is calculated by adding the variances of data noise, which in turn is inversely proportional to the number of quanta that are registered. The key to understanding noise reduction by

redistribution of intensities is given by the known dependency of noise on the number of registered quanta N. The standard deviation behaves like $1/\sqrt{N}$. For small N, the function $1/\sqrt{N}$ changes rapidly, but less so for large N. Equal differences in the number of quanta, therefore, have different impact on the resulting image noise. Reducing the number of quanta in projections with low attenuation and hence large number of quanta will influence noise in these projections only slightly while redistributing these quanta to projections with high attenuation and hence low number of detected quanta may reduce noise there in a comparatively drastic manner. Of course, we can redistribute only the emitted and not the directly registered quanta. As a result, shifting quanta from low- to high-attenuation views will lower the overall number of registered quanta. Yet, the redistribution will result in an overall image noise reduction. The optimum will be achieved when the primary intensity is shifted from constant to weighted by the square root of attenuation. It is tempting to assume that the optimum is given when modulating according to attenuation directly, i.e., when all registered N_i are equal. However, this would ignore the fact that the total number of quanta N_0 is held constant. This dependence is very well demonstrated by the simulated images as a function of the control parameter α (Figs. 10–12).

V. CONCLUSION

The simulation studies confirm the theoretical prediction that dose control by tube current modulation has a great potential to either improve image quality through noise reduction, or to reduce radiation exposure without impairing image quality.

Using a fixed shape sinusoidal modulation function for tube current yields a smaller effect in dose reduction than can be obtained by attenuation-based current modulation (Table II). Moreover, sufficient amplitudes in tube current modulation are necessary to be able to realize the optimal degree of noise reduction. Should a limiting amplitude for tube current modulation be reached before dose control strength has reached the optimal value of 0.5, then only part of the potential dose reduction is achieved.

Another benefit associated with dose control apart from either reducing noise or dose is the possibility to influence the homogeneity of the image noise structure as is demonstrated by Figs. 10–12.

A second part of this work will verify the results on physical phantoms.

[a]Author to whom correspondence should be addressed. Also at: Institute of Medical Physics, University of Erlangen, Krankenhausstr. 12, D-91054 Erlangen, Germany. Telephone: 011-49-9131-8522310; Fax: 011-49-9131-8522824; Electronic mail: willi@imp.uni-erlangen.de

[1]L. N. Rothenberg and K. S. Pentlow, ''Radiation dose in CT,'' Radiographics **12**(6), 1225–43 (1992).

[2]J. Bernhardt, R. Veit, and B. Bauer, ''Erhebungen zur Strahlenexposition der Patienten bei der Röntgendiagnostik,'' Z. Med. Phys. **5**, 33–39 (1995).

[3]I. R. Kamel, J. E. Hernandez, A. E. Martin, A. E. Schlesinger, K. E. Niklason, and K. E. Guire, ''Radiation dose reduction in CT of the pediatric pelvis,'' Radiology **190**(3), 683–687 (1994).

[4]A. G. Jurik, K. A. Jessen, and J. Hansen, ''Image quality and dose in computed tomography,'' Eur. Radiol. **7**(1), 77–81 (1997).

[5]F. R. Verdun, F. O. Meuli, F. O. Bochud, C. Imsand, S. Raimondi, P. Schnyder, and J.-F. Valley, ''Image quality and dose in spiral computed tomography,'' Eur. Radiol. **6**(4), 485–488 (1996).

[6]D. A. Chesler, S. J. Riederer, and N. J. Pelc, ''Noise due to photon counting statistics in computed x-ray tomography,'' J. Comput. Assist. Tomogr. **1**, 64–74 (1977).

[7]J. R. Haaga, F. Miraldi, W. McIntyre, J. P. LiPuma, P. J. Bryan, and E. Wiesen, ''The effect of mAs variation upon computed tomography image quality as evaluated *in vivo* and *in vitro* studies,'' Radiology **138**, 449–454 (1981).

[8]Edited by GE Medical Systems, ''CT Hispeed Advantage RP System,'' GE Technical Publications **15**, 12–20 (1994).